Hybrid tandem quantum dot/organic photovoltaic cells with complementary near infrared absorption

Taesoo Kim, Elenita Palmiano, Ru-Ze Liang, Hanlin Hu, Banavoth Murali, Ahmad R. Kirmani, Yuliar Firdaus, Yangqin Gao, Arif Sheikh, Mingjian Yuan, Omar F. Mohammed, Sjoerd Hoogland, Pierre M. Beaujuge, Edward H. Sargent, and Aram Amassian

Citation: Appl. Phys. Lett. **110**, 223903 (2017); doi: 10.1063/1.4984023

View online: http://dx.doi.org/10.1063/1.4984023

View Table of Contents: http://aip.scitation.org/toc/apl/110/22

Published by the American Institute of Physics

Hybrid tandem quantum dot/organic photovoltaic cells with complementary near infrared absorption

Taesoo Kim,[1] Elenita Palmiano,[2] Ru-Ze Liang,[1] Hanlin Hu,[1] Banavoth Murali,[1,a)] Ahmad R. Kirmani,[1] Yuliar Firdaus,[1] Yangqin Gao,[1] Arif Sheikh,[1] Mingjian Yuan,[2] Omar F. Mohammed,[1] Sjoerd Hoogland,[2] Pierre M. Beaujuge,[1] Edward H. Sargent,[2] and Aram Amassian[1,b)]

[1]*King Abdullah University of Science and Technology (KAUST), KAUST Solar Center (KSC), and Physical Science and Engineering Division, Thuwal 23955-6900, Saudi Arabia*

[2]*Department of Electrical and Computer Engineering, University of Toronto, Toronto, Ontario M5S 3G4, Canada*

(Received 1 March 2017; accepted 10 May 2017; published online 1 June 2017)

Monolithically integrated hybrid tandem solar cells that effectively combine solution-processed colloidal quantum dot (CQD) and organic bulk heterojunction subcells to achieve tandem performance that surpasses the individual subcell efficiencies have not been demonstrated to date. In this work, we demonstrate hybrid tandem cells with a low bandgap PbS CQD subcell harvesting the visible and near-infrared photons and a polymer:fullerene—poly (diketopyrrolopyrrole-terthiophene) (PDPP3T):[6,6]-phenyl-C_{60}-butyric acid methyl ester ($PC_{61}BM$)—top cell absorbing effectively the red and near-infrared photons of the solar spectrum in a complementary fashion. The two subcells are connected in series via an interconnecting layer (ICL) composed of a metal oxide layer, a conjugated polyelectrolyte, and an ultrathin layer of Au. The ultrathin layer of Au forms nano-islands in the ICL, reducing the series resistance, increasing the shunt resistance, and enhancing the device fill-factor. The hybrid tandems reach a power conversion efficiency (PCE) of 7.9%, significantly higher than the PCE of the corresponding individual single cells, representing one of the highest efficiencies reported to date for hybrid tandem solar cells based on CQD and polymer subcells. *Published by AIP Publishing.* [http://dx.doi.org/10.1063/1.4984023]

Solution-processed thin film solar cells based on colloidal quantum dot (CQD) and organic light absorbers are compatible with low-cost, large-area manufacturing processes amenable to efficient, lightweight modules.[1–4] In recent years, both CQD and organic photovoltaic devices have seen significant efficiency improvements, with single-junction devices reaching power conversion efficiencies (PCE) of over 12%.[5–8] In theory, multi-junction solar cell devices can harvest a broader portion of the solar spectrum and, in turn, are of interest to achieve higher open-circuit voltage (V_{OC}) and PCE values via subcells electrically connected in series by an interconnecting layer (ICL).[9–13] CQDs benefit from a size-tunable bandgap that allows absorption of photons with a relatively wide range of wavelengths but a weaker absorption in the red and near-infrared (NIR) regions of the solar spectrum.[3,7,8] Meanwhile, organic absorbers can have a narrower and more tunable spectral absorption than that of CQDs, making organic subcells especially attractive for tandem and triple-junction solar cells.[14–16] CQD tandem solar cells have received limited attention thus far, that is, a handful of all-CQD tandem solar cells have been reported with a open circuit voltage (V_{OC}) ideally equal to the sum of the V_{OC} values of the two subcells (i.e., ~1.0 V). In addition, CQD tandems tend to yield only modest efficiency enhancements relative to their single-cell counterparts, mainly because of their modest fill-factors (FFs) (typically < 50%) and the limited photocurrent related to the relatively weak photon absorption near the CQD band edge.[3,7,8,12,13] In contrast, all-organic tandem solar cells have the benefit of achieving both high V_{OC} (i.e., > 1.5 V) and FF (i.e., > 65%).[14–16] Therefore, the opportunity exists to expand beyond the spectral range of individual quantum-dot and organic absorbers by combining the two material types into a hybrid tandem solar cell which can overcome the present limitations of both CQD homo-tandems and polymer homo-tandems.

In this letter, we report on a hybrid tandem solar cell that combines a low bandgap bulk heterojunction polymer:fullerene subcell with a PbS CQD subcell.[3,17–19] The combination of a low bandgap polymer donor with [6,6]-phenyl-C_{60}-butyric acid methyl ester ($PC_{61}BM$), selected as the acceptor because of its weak absorption in the visible, ensures excellent spectral complementarity with the CQD subcell in the visible and near infrared (NIR) regions of the solar spectrum. In turn, the PCE of the hybrid tandem is found to improve significantly from the previously reported value of 5.3% to the value of 7.9%, using a similar device architecture.[15,19] The monolithically integrated tandem is electrically connected in series using p- and n-type interconnecting layers (ICLs) that combine a metal oxide and a conjugated polyelectrolyte sandwiching an ultrathin and unpercolated Au layer forming isolated nanoislands.[20–23] The tandem device achieves a high V_{OC} (1.25 V) equal to the sum of the subcell voltages and a high FF (67%), indicating that the subcells are properly connected via the ICL. The

a)Current address: School of Chemistry, University of Hyderabad, 500046 Telangana State, India

b)Author to whom correspondence should be addressed: aram.amassian@kaust.edu.sa

hybrid tandem PCE of 7.9% is one of the highest efficiencies reported to date in hybrid tandem solar cells combining CQD and organic subcells.[19,24,25] It surpasses both the efficiencies of the organic single cell (6.6%) and that of the CQD single cell (4.8%).

In Figure 1(a), we show the material systems used in this study: a PbS quantum dot with an organic 3-mercaptopropionic acid (MPA) ligand for the bottom cell,[18,26] as well as the chemical structures of the polymer donor and acceptor included in the top cell.[15,22,27,28] The high-resolution transmission electron microscopy (TEM) image of PbS quantum dots before the ligand exchange is shown in Figure S1 (supplementary material): the CQD size is ca. 3 nm matched with the size (d) - bandgap (E_0) equation suggested by Moreels *et al.*,[29] $E_0 = 0.41 + 1/(0.0252d^2 + 0.283d)$. The polymer donor poly (diketopyrrolopyrrole-terthiophene) (PDPP3T) used in conjunction with the fullerene acceptor [6,6]-phenyl-C_{60}-butyric acid methyl ester ($PC_{61}BM$) forms the organic bulk heterojunction subcell.[15,22,27,28] The conjugated polyelectrolyte, poly[(9,9-bis(3′-(N,N-dimethylamino)propyl)-2,7-fluorene)-alt-2,7-(9,9-dioctylfluorene)] (PFN), is used as a n-type layer in the ICL.[23] In Figure 1(b), we show the absorption spectra of the PbS CQD and PDPP3T:$PC_{61}BM$ active layers, with film thicknesses of 125 nm and 130 nm, respectively, as measured using a surface profilometer. These thicknesses were chosen for optimal absorption of the incoming photons to facilitate current matching conditions. The CQD active layer has a wide absorption spectrum covering the visible and NIR regions with a first excitation peak at 925 nm.[29] The CQD layer shows relatively strong absorption in the short-wavelength visible range and weaker absorption in the red and NIR, while the PDPP3T:$PC_{61}BM$ subcell transmits the visible spectrum until around 550 nm and then absorbs effectively in the red and NIR regions (up to 900 nm). The spectral responses of the two active layers are thus complementary: the PbS CQD layer contributes more to the absorption of the shorter-wavelength visible region with some contribution at the longer wavelengths, while the PDPP3T:$PC_{61}BM$ active layer compensates for the CQD layer's weaker absorption in the red and NIR regions. The detailed description of active layer preparation by solution-processing and the fabrication methods of the single and tandem devices are summarized in the supplementary material.

In Figure 1(c), we illustrate the hybrid tandem device configuration composed of bottom PbS CQD and top PDPP3T:$PC_{61}BM$ subcells. The PbS CQD active layer was spin-coated on aluminum-doped zinc oxide (AZO) coated on ITO-coated glass substrates using a 3-mercaptopropionic acid (MPA) ligand exchange protocol in acetonitrile (ACN).[18,26] As a solvent of the CQD solution, hexane with the low boiling point (b.p.) of 68 °C was used instead of octane (b.p.: 125 °C) to form a thicker CQD layer in a single solution-casting step. The ICL consists of a stack of MoO_3/thin Au/PFN, with MoO_3 vacuum-deposited to form a p-type hole transporting layer (HTL), on top of which a thin Au layer (1 nm) was deposited by thermal evaporation with accurate thickness monitoring, and without the use of a wetting layer to promote islanding of Au.[20–23] The performance of the hybrid tandem solar cells was found to be strongly impacted by the presence of the Au nano-islands, as will be discussed below in detail. The conjugated polyelectrolyte PFN was spin-coated on top of the stack to form the n-type electron transporting layer (ETL). The PDPP3T:$PC_{61}BM$ layer was deposited on top of the ICL by spin-coating. The tandem stack was completed by vacuum evaporation of MoO_3 as HTL and Ag as the anode. The energy diagram of the hybrid tandem device stack is schematically illustrated in Figure 1(d).[12,27]

In Figure 2(a), we show the representative current density-voltage (J-V) characteristics obtained for the individual single-junction cells and the optimized hybrid tandem cell. In these devices, the active layers had thicknesses of

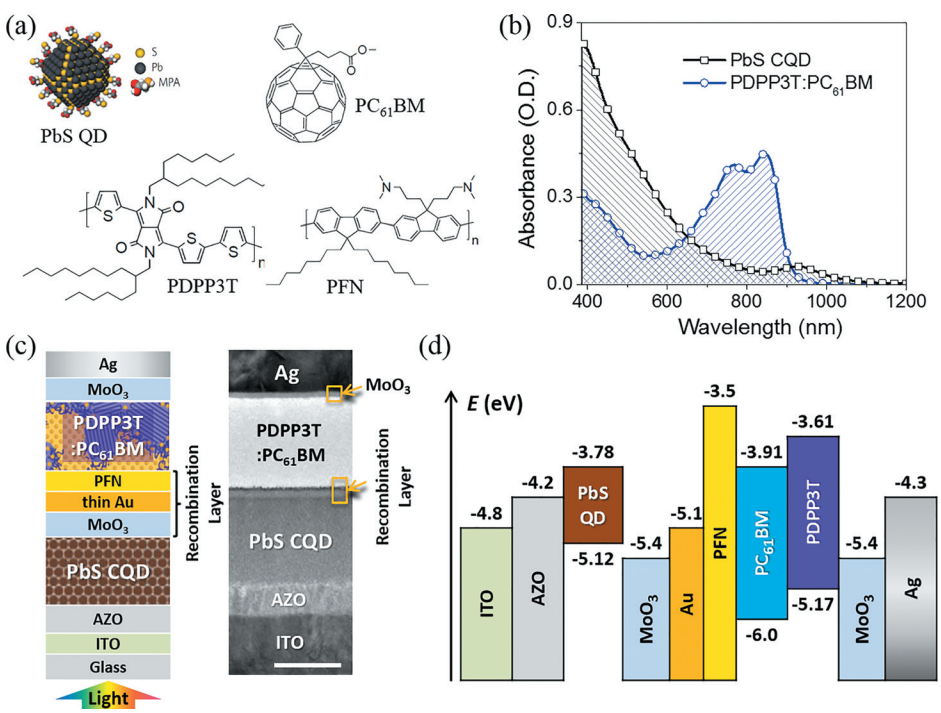

FIG. 1. (a) Materials chart, including PbS quantum dot after ligand exchange, the polymer donor PDPP3T, $PC_{61}BM$ as the fullerene acceptor, and the conjugated polyelectrolyte PFN. (b) Absorbance spectra of the PbS CQD and the PDPP3T:$PC_{61}BM$ active layers. (c) Hybrid tandem solar cell configuration and TEM cross-sectional image of the corresponding device. The scale bar is 100 nm. (d) Energy diagram of the hybrid tandem solar cell.

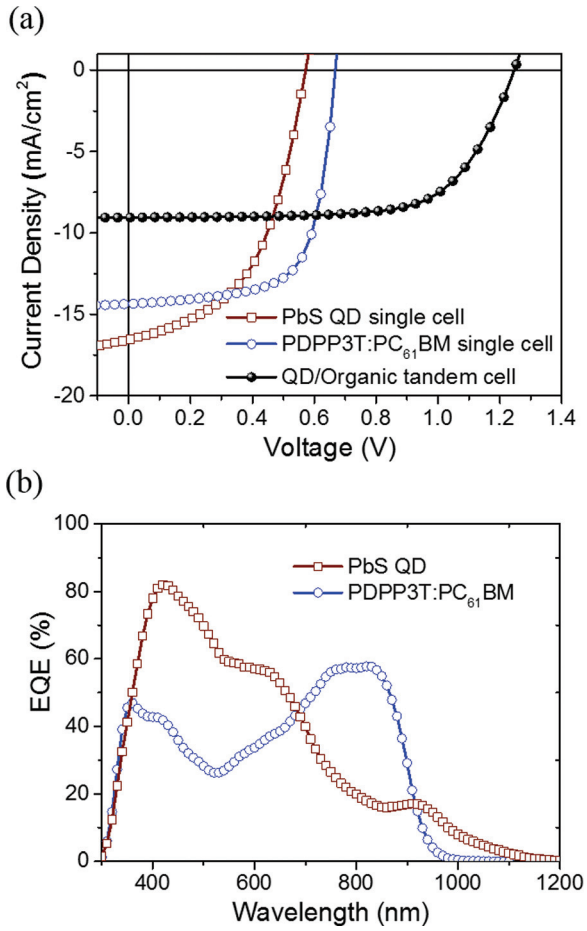

FIG. 2. (a) *J-V* curves of the single-junction and hybrid tandem cells and (b) EQE spectra of the CQD and PDPP3T:PC$_{61}$BM single-junction cells.

125 nm and 130 nm. Optical simulations of sub-cell thickness based on the transfer matrix formalism helped identify these active layer thicknesses which achieve the maximum current density in the tandem solar cell (Figure S2, supplementary material). We utilized these conditions to fabricate the tandem solar cells and found the tandem devices to yield the reported device performance, which surpasses the performance of individual sub-cells.

The device configuration of the PbS QD single cell is glass/ITO/AZO/PbS CQD/MoO_3/Au/Ag, which on average yielded an open circuit voltage (V_{OC}) of 0.57 V, a short circuit current (J_{SC}) of 16.3 mA/cm^2, and a fill factor (FF) of 50.4%, resulting in a PCE of 4.7% (Table I). The configuration of the inverted organic single cell is glass/ITO/PFN/PDPP3T:PC$_{61}$BM/MoO_3/Ag, which on average yielded a V_{OC} of 0.67 V, a J_{SC} of 14.3 mA/cm^2, a FF of 67.8%, and a PCE of 6.5%. This performance was slightly better than devices made with a thicker active layer (Table I), mainly due to the better FF for the thinner devices. Standard deviations of device parameters are summarized in Table SI (supplementary material).

The external quantum efficiency (EQE) for the single-junction QD and polymer cells is presented in Figure 2(b). The CQD cell harvests effectively in the short-wavelengths region of the solar spectrum (blue region), but the EQE drops rapidly from ca. 650 nm all the way to the band edge at ca. 1100 nm. In the red and near infrared (NIR) regions, for $\lambda > 650$ nm, the EQE of the PDPP3T:PC$_{61}$BM cell is particularly pronounced. The hybrid tandem solar cell with these subcells shows a FF of 67.2%, leading to a PCE of 7.7% on average and a best PCE value of 7.9%. The hybrid tandem solar cells exhibit higher PCE than the single cells made of the individual active layers. This result suggests that the active layers of complementary absorption spectra are efficiently connected via the ICL when the ultrathin Au layer is included in the hybrid tandem device configuration. We tested the shelf life of the PbS sub-cell, the organic sub-cell, and the hybrid tandem cell after storage in a nitrogen glovebox for 3 months without additional device encapsulation (Figure S3, supplementary material). The hybrid tandem cells retained >70% of the original PCE and appears to be more stable than the QD sub-cell, which retains ca. 66% of its PCE, but less than the organic sub-cell. This shows that the hybrid tandem consisting of an organic sub-cell fabricated over the QD sub-cell may offer the latter some protection from degradation.

Appropriate energy level alignment in the interconnecting layer is crucial to ensure that carriers are appropriately transported to the ICL where they must effectively recombine. The energy level offset between the n- and p-type layers was reduced by inserting an ultrathin Au layer,[13,20–22] which forms disconnected Au nanoislands on MoO_3, as shown in the inset of Figure 3(a) and Figure S4 (supplementary material). This approach has been shown to work in various tandem solar cells,[13,20–22] leading to the formation of an asymmetric work function within the ICL which yields a graded work-function with a high work-function towards the CQD bottom subcell for hole extraction and a low work-function towards the polymer top cell for electron extraction.[30] It is worth noting that the hybrid tandem device reached a V_{OC} of 1.2 V irrespective of thin Au layer insertion into the ICL. However, the FF of the hybrid tandem devices significantly improved with Au layer insertion (Table I and Figure 3(a): the thickness of each of the CQD and active

TABLE I. Device parameters of the PbS CQD and PDPP3T:PC$_{61}$BM single-junction cells and those of the hybrid tandem solar cells without (w/o) and with (w/) ultrathin Au layer included in the ICL. Standard deviations of the device parameters are summarized in Table SI (supplementary material).

Device structure	Active layer	Thick	ICL	V_{OC} (V)	J_{SC} (mA/cm^2)	FF (%)	PCE (%)	Best PCE (%)
Single cell	PbS CQD	125 nm	…	0.57	16.3	50.4	4.7	4.8
	PDPP3T:PC$_{61}$BM	140 nm	…	0.67	14.6	64.5	6.3	6.4
	PDPP3T:PC$_{61}$BM	130 nm	…	0.67	14.3	67.8	6.5	6.6
Tandem cell	PbS CQD/PDPP3T:PC$_{61}$BM	125 nm /140 nm	w/o Au	1.23	9.3	57.6	6.6	6.7
		125 nm /140 nm	w/Au	1.24	9.4	63.2	7.4	7.4
		125 nm /130 nm	w/Au	1.25	9.3	67.2	7.7	7.9

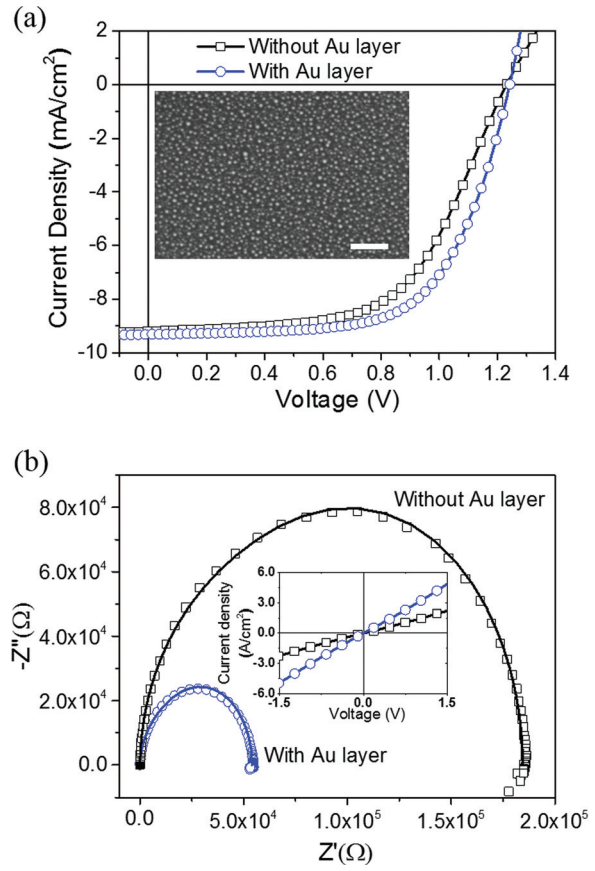

FIG. 3. Influence of Au nano-islands within the ICL: (a) *J-V* curves of hybrid tandem cells. The inset shows the nanometer sized Au islands on the MoO_3 layer; the scale bar is 100 nm and (b) Impedance spectra of the tandem solar cells under illumination. Solid lines show the fits. The inset shows the conductance of the ICL with the device structure of ITO glass/MoO_3/ without or with thin Au/PFN/Ag.

organic layers is 125 nm and 140 nm, respectively, in this case.). The higher FF is attributed to the efficient recombination of the electrons and holes at the MoO_3/PFN interface enabled by the presence of Au nanoislands. The latter act as efficient recombination sites in the ICL, resulting in less accumulation of photo-excited charges in the active layer and interfaces.[13,20–22] It reduces the contact resistance, resulting in reduced series resistance (at $V = V_{OC}$) and higher shunt resistance (at $V = 0$) than in tandems which do not use a thin Au layer (Table SI, supplementary material).[13,20–22] We also used electrical impedance spectroscopy (EIS) to investigate the impact of the Au islands in the ICL on the performance of the tandem solar cells.[31,32] In Figure 3(b), we show the Cole-Cole plot (the imaginary impedance Z'' over the real impedance Z') of the tandem devices under illumination. The plot reveals that the charge transport resistance in the ICL is lower in the presence of Au nano-islands, which is consistent with the conductance measurements shown in the inset of Figure 3(b). The conductance measurements were performed on the isolated interlayer stacks, namely, glass/ITO/MoO_3/PFN/Ag and glass/ITO/MoO_3/thin Au/PFN/Ag devices.[13] The results show that the Au nanoislands reduce the series resistance even though both interlayer stacks exhibited Ohmic characteristics.[13,20]

In summary, we demonstrated a hybrid tandem solar cell combining solution-processed PbS CQD and PDPP3T:$PC_{61}BM$ subcells exhibiting complementary spectral absorption in the visible and near infrared parts of the solar spectrum. The insertion of ultrathin Au layers (composed of nanoislands) into the MoO_3/PFN interconnection layer reduces the series resistance and increases the shunt resistance of the tandem device stacks, resulting in increased FF and PCEs with up to 7.9% achieved upon careful device optimization. This tandem structure surpasses the efficiency of individual single cells and is one of the highest efficiencies reported to date for hybrid tandem solar cells combining CQD and polymer subcells.

See supplementary material for the device fabrication method and characterization.

This work was supported by the King Abdullah University of Science and Technology (KAUST). Part of this work was supported by the Competitive Research Grant (round 2, KAUST) and by the KAUST Solar Center's Competitive Research Fund (Project C3). E.H.S. acknowledges funding from the Ontario Research Fund.

[1]A. J. Heeger, Adv. Mater. **26**, 10–28 (2014).
[2]L. Dou, J. You, Z. Hong, Z. Xu, G. Li, R. A. Street, and Y. Yang, Adv. Mater. **25**, 6642–6671 (2013).
[3]J. Y. Kim, O. Voznyy, D. Zhitomirsky, and E. H. Sargent, Adv. Mater. **25**, 4986–5010 (2013).
[4]B. I. MacDonald, A. Martucci, S. Rubanov, S. E. Watkins, P. Mulvaney, and J. J. Jasieniak, ACS Nano **6**, 5995–6004 (2012).
[5]S. Li, L. Ye, W. Zhao, S. Zhang, S. Mukherjee, H. Ade, and J. Hou, Adv. Mater. **28**, 9423–9429 (2016).
[6]D. Baran, R. S. Ashraf, D. A. Hanifi, M. Abdelsamie, N. Gasparini, J. A. Röhr, S. Holliday, A. Wadsworth, S. Lockett, M. Neophytou, C. J. M. Emmott, J. Nelson, C. J. Brabec, A. Amassian, A. Salleo, T. Kirchartz, J. R. Durrant, and I. McCulloch, Nat. Mater. **16**, 363–369 (2017).
[7]C.-H. M. Chuang, P. R. Brown, V. Bulović, and M. G. Bawendi, Nat. Mater. **13**, 796–801 (2014).
[8]M. Liu, O. Voznyy, R. Sabatini, F. P. García de Arquer, R. Munir, A. H. Balawi, X. Lan, F. Fan, G. Walters, A. R. Kirmani, S. Hoogland, F. Laquai, A. Amassian, and E. H. Sargent, Nat. Mater. **16**, 258–263 (2017).
[9]J. Y. Kim, K. Lee, N. E. Coates, D. Moses, T. Q. Nguyen, M. Dante, and A. J. Heeger, Science **317**, 222–225 (2007).
[10]A. Hadipour, B. de Boer, and P. W. M. Blom, Adv. Funct. Mater. **18**, 169–181 (2008).
[11]L. Dou, J. You, J. Yang, C.-C. Chen, Y. He, S. Murase, T. Moriarty, K. Emery, G. Li, and Y. Yang, Nat. Photonics **6**, 180–185 (2012).
[12]X. Wang, G. I. Koleilat, J. Tang, H. Liu, I. J. Kramer, R. Debnath, L. Brzozowski, D. A. R. Barkhouse, L. Levina, S. Hoogland, and E. H. Sargent, Nat. Photonics **5**, 480–484 (2011).
[13]J. J. Choi, W. N. Wenger, R. S. Hoffman, Y.-F. Lim, J. Luria, J. Jasieniak, J. A. Marohn, and T. Hanrath, Adv. Mater. **23**, 3144–3148 (2011).
[14]Y. Gao, V. M. Le Corre, A. Gaïtis, M. Neophytou, M. A. Hamid, K. Takanabe, and P. M. Beaujuge, Adv. Mater. **28**, 3366–3373 (2016).
[15]W. Li, A. Furlan, K. H. Hendriks, M. M. Wienk, and R. A. J. Janssen, J. Am. Chem. Soc. **135**, 5529–5532 (2013).
[16]C.-C. Chen, W.-H. Chang, K. Yoshimura, K. Ohya, J. You, J. Gao, Z. Hong, and Y. Yang, Adv. Mater. **26**, 5670–5677 (2014).
[17]A. G. Pattantyus-Abraham, I. J. Kramer, A. R. Barkhouse, X. Wang, G. Konstantatos, R. Debnath, L. Levina, I. Raabe, M. K. Nazeeruddin, M. Gratzel, and E. H. Sargent, ACS Nano **4**, 3374–3380 (2010).
[18]A. R. Kirmani, G. H. Carey, M. Abdelsamie, B. Yan, D. Cha, L. R. Rollny, X. Cui, E. H. Sargent, and A. Amassian, Adv. Mater. **26**, 4717–4723 (2014).
[19]T. Kim, Y. Gao, H. Hu, B. Yan, Z. Ning, L. K. Jagadamma, K. Zhao, A. R. Kirmani, J. Eid, M. M. Adachi, E. H. Sargent, P. M. Beaujuge, and A. Amassian, Nano Energy **17**, 196–205 (2015).
[20]A. Martínez-Otero, Q. Liu, P. Mantilla-Perez, M. M. Bajo, and J. Martorell, J. Mater. Chem. A **3**, 10681–10686 (2015).
[21]Z. Zheng, S. Zhang, M. Zhang, K. Zhao, L. Ye, Y. Chen, B. Yang, and J. Hou, Adv. Mater. **27**, 1189–1194 (2015).
[22]D. Gupta, M. M. Wienk, and R. A. J. Janssen, ACS Appl. Mater. Interfaces **6**, 13937–13944 (2014).

[23]Z. He, C. Zhong, S. Su, M. Xu, H. Wu, and Y. Cao, Nat. Photonics **6**, 593–597 (2012).
[24]M. J. Speirs, B. G. H. M. Groeneveld, L. Protesescu, C. Piliego, M. V. Kovalenko, and M. A. Loi, Phys. Chem. Chem. Phys. **16**, 7672 (2014).
[25]H. Aqoma, R. Azmi, S.-H. Oh, and S.-Y. Jang, Nano Energy **31**, 403–409 (2017).
[26]A. H. Ip, S. M. Thon, S. Hoogland, O. Voznyy, D. Zhitomirsky, R. Debnath, L. Levina, L. R. Rollny, G. H. Carey, A. Fischer, K. W. Kemp, I. J. Kramer, Z. Ning, A. J. Labelle, K. W. Chou, A. Amassian, and E. H. Sargent, Nat. Nanotechnol. **7**, 577–582 (2012).
[27]J. C. Bijleveld, A. P. Zoombelt, S. G. J. Mathijssen, M. M. Wienk, M. Turbiez, D. M. de Leeuw, and R. A. J. Janssen, J. Am. Chem. Soc. **131**, 16616–16617 (2009).
[28]J. Wang, F. Zhang, M. Zhang, W. Wang, Q. An, L. Li, Q. Sun, W. Tang, and J. Zhang, Phys. Chem. Chem. Phys. **17**, 9835–9840 (2015).
[29]I. Moreels, K. Lambert, D. Smeets, D. De Muynck, T. Nollet, J. C. Martins, F. Vanhaecke, A. Vantomme, C. Delerue, G. Allan, and Z. Hens, ACS Nano **3**, 3023–3030 (2009).
[30]Y. Liu, L. A. Renna, M. Bag, Z. A. Page, P. Kim, J. Choi, T. Emrick, D. Venkataraman, and T. P. Russell, ACS Appl. Mater. Interfaces **8**, 7070–7076 (2016).
[31]Y. Chen, W.-C. Lin, J. Liu, and L. Dai, Nano Lett. **14**, 1467–1471 (2014).
[32]J. H. Seo, D. H. Kim, S. H. Kwon, M. Song, M. S. Choi, S. Y. Ryu, H. W. Lee, Y. C. Park, J. D. Kwon, K. S. Nam, Y. Jeong, J. W. Kang, and C. S. Kim, Adv. Mater. **24**, 4523–4527 (2012).